Journal of Translational Medicine

RESEARCH

Open Access

The biomarker potential of circPOLD1 and its binding protein YBX1 in cervical carcinogenesis

Lu Zhao[1†], Xin Chen[2†], Yanan Zhang[1,3†], Yixuan Cen[1], Tingjia Zhu[2], Lingfang Wang[2], Lili Xia[1], Yang Li[1], Xiaodong Cheng[1], Xing Xie[1^], Weiguo Lu[1,4*] and Junfen Xu[1,2*]

Abstract

Background Cervical cancer progresses through distinct precancerous stages, making early screening and intervention crucial for prevention. However, conventional screening modalities, such as cytology and HPV testing, face challenges related to sensitivity, specificity, and resource dependency. Circular RNAs (circRNAs), owing to their high stability and tissue-specific expression, have emerged as promising biomarkers, though their role in cervical carcinogenesis remains underexplored. In particular, the clinical utility of circRNAs for optimizing cervical cancer screening and early diagnosis has yet to be established. This study aimed to investigate the dynamic expression profiles of circRNAs across various stages of cervical cancer progression and identify potential biomarkers to enhance early detection.

Methods CircRNA sequencing was performed on cervical tissues spanning normal cervical epithelium (NCE), high-grade squamous intraepithelial lesions (HSIL), and cervical squamous cell carcinoma (CSCC). Functional assays, including cell viability, colony formation, and apoptosis, were performed to assess the oncogenic potential of circPOLD1 and its interaction with YBX1 in cervical cancer cells. BaseScope and immunohistochemistry (IHC) were applied to tissue microarrays for clincial validation and ROC curve analysis evaluated the diagnostic performance of circPOLD1 in serum as a liquid biopsy marker.

Results CircRNA profiling revealed a progressive increase in circPOLD1 expression from NCE to HSIL and CSCC. Mechanistically, circPOLD1 functioned as an oncogene by binding to and phosphorylating YBX1, activating the AKT/mTOR/HIF-1α pathway to enhance glycolysis-driven tumorigenesis. BaseScope and IHC confirmed the stage-specific elevation of circPOLD1 and YBX1 in cervical lesions. The circPOLD1/YBX1 multi-marker panel demonstrated superior diagnostic performance, achieving an AUC of 0.951 for LSIL+ and 0.817 for HSIL+ detection. Furthermore, serum circPOLD1 levels exhibited a progressive increase across disease stages, underscoring its potential as a non-invasive biomarker.

Conclusion circPOLD1 and YBX1 synergistically drive cervical carcinogenesis and exhibit stage-specific expression patterns. Their combined detection significantly enhanced the accuracy for cervical cancer screening and dynamic monitoring. The successful application of BaseScope and IHC highlights the immediate translational potential of these

[†]Lu Zhao, Xin Chen and Yanan Zhang equally contributed to this work.

[^]Xing Xie was deceased on April 3, 2023.

*Correspondence:
Weiguo Lu
lbwg@zju.edu.cn
Junfen Xu
xjfzu@zju.edu.cn
Full list of author information is available at the end of the article

biomarkers, paving the way for refined risk stratification, improved therapeutic targeting, and reduced cervical cancer burden through early intervention.

Keywords Cervical cancer, circPOLD1, YBX1, Biomarker, Screening

Introduction

Cervical cancer remains the fourth most common malignancy in women globally, with an estimated 661,000 new cases and 348,000 deaths annually [1]. Its pathogenesis is characterized by a multistep progression, where persistent HPV infection leads to precancerous lesions, which may progress to invasive carcinoma [2]. Early intervention through the screening and treatment of precancerous lesions is key to preventing cervical cancer, making early detection methods critically important. However, current screening approaches such as the ThinPrep Cytologic Test (TCT) and HPV testing face significant challenges, including issues of sensitivity, specificity, and resource dependency. The accuracy of TCT is affected by sampling quality and cytopathologist expertise, with a sensitivity of around 65% [3, 4]. Although HPV testing offers high sensitivity, its limited specificity makes it difficult to distinguish between transient and persistent infections, with 90% of HPV16/18 infections resolving spontaneously within 2 years [5, 6], leading to unnecessary colposcopy referrals and biopsies [7]. In resource-limited settings, accessibility, cost, and patient compliance further hinder effective screening. Therefore, there is an urgent need to explore molecular biomarkers for optimizing early screening and diagnosis of cervical cancer and its precursors.

Recent advances in molecular techniques, including methylation test [8], HPV integration detection [9], and microRNA profiling [10], have shown promise for improving cervical cancer diagnostics. However, DNA methylation and HPV integration detection face technical challenges and high costs, and DNA methylation assays have shown suboptimal sensitivity (63% for CIN2 and 71% for CIN3 detection) [11]. Additionally, the instability and low abundance of miRNA limit their clinical application. These limitations underscore the need for more reliable, cost-effective biomarkers with improved detection precision.

Circular RNA (circRNA) represent a novel class of non-coding RNA characterized by their covalently closed loop structure. This unique feature confers exceptional stability, making circRNAs highly resistant to degradation by ribonucleases, which is an advantageous trait for biomarker development [12, 13]. CircRNAs are evolutionarily conserved and exhibit tissue-specific expression patterns, making them promising candidates for cancer biomarkers [14–19]. Recent studies have identified circRNAs as key regulators in various cancers, with circRNAs functioning through diverse mechanisms, including acting as microRNA sponges, binding to RNA-binding proteins, modulating transcription factors, and even participating in protein translation [20, 21]. For instance, circ_0001589 has been shown to promote cervical cancer progression by enhancing HMGB1 expression [22], while circSTX6 regulates cervical carcinogenesis by stabilizing SP1 [23]. Despite these insights, the role of circRNAs in the progressive stages of cervical carcinogenesis has not been fully explored. Specifically, the stage-specific expression and diagnostic potential of circRNAs in cervical cancer remain to be clarified.

In this study, we aim to profile the dynamic expression of circRNAs across different stages of cervical cancer progression, including normal cervical epithelium (NCE), high-grade squamous intraepithelial lesions (HSIL), and cervical squamous cell carcinoma (CSCC). We focus on identifying a stage-specific circRNA and investigating its mechanistic role in cervical carcinogenesis. Additionally, we explore the potential of circRNAs as diagnostic biomarkers for early cervical cancer detection through serum analysis and tissue-based assays. By utilizing BaseScope in situ hybridization assay and immunohistochemistry (IHC) to validate these findings in tissue samples, we provide crucial insights into circRNA-mediated oncogenic pathways. This study highlights the translational potential of circRNAs for enhancing early detection, guiding therapeutic interventions, and improving clinical outcomes in cervical cancer.

Results

The profiles and identification of differentially expressed circRNAs in cervical squamous-cell carcinoma and precursor tissues

To explore the circRNA expression profiles in cervical cancer and precursor, we performed RNA sequencing analysis with ribosomal RNA-depleted in HPV-NCE, HPV16 + NCE, HPV16 + HSIL, and HPV16+ CSCC tissues (n = 6/each group). The box plot of the FPKM of 24 sequencing samples showed good reproducibility among the biological repetitions (Fig. 1A). Totally 66,868 circRNAs were identified (Back-spliced junctions reads ≥ 1), the detailed data of which were available in GEO database (GSE147009), of those, 17,732 circRNAs were available in CircBase database. The numbers of identified circRNAs and the source of reads sequences containing

circRNA back-spliced site were similar among HPV16− NCE, HPV16+ NCE, HSIL and CSCC tissue samples.

To identify oncogenic circRNAs in the initiation process of cervical cancer, the differentially expressed circRNAs were analyzed. The numbers of differentially expressed circRNAs among HPV-NCE, HPV16+ NCE, HSIL, and CSCC tissues were showed in the histogram (Fig. 1B). Differentially expressed circRNAs between HSIL and HPV-NCE, CSCC and HPV-NCE, HSIL and HPV16+ NCE, CSCC and HPV16+ NCE, HPV16+ NCE and HPV-NCE, as well as CSCC and HSIL, were shown in volcano plot figures (Fig. 1C–H). In this study, we focused on the up-regulated circRNAs in HSIL and CSCC compared with HPV− or HPV16+ NCE to seek potential circRNA biomarkers for cervical cancer screening. Compared with HPV-NCE tissues, totally 70 and 246 circRNAs were up-regulated in HSIL and CSCC, respectively, among them, nine circRNAs were up-regulated in both HSIL and CSCC tissues (Fig. 1I). While compared with HPV16+ NCE tissues, only one circRNA was up-regulated in both HSIL and CSCC tissues (Fig. 1J), which was just included in above nine circRNAs up-regulated in both HSIL and CSCC compared with HPV-NCE. Thus, we designed junction-specific divergent primers of nine circRNAs, respectively, but only three primers (circRP13-279N23.2, circSTAG1, and circPOLD1) could produce stable and specific products for further study.

Validation of differentially expressed circRNAs in cervical squamous-cell carcinoma and precursor tissues

The expression of circRP13-279N23.2, circSTAG1, and circPOLD1 was validated by qRT-PCR in HPV-NCE (n = 32), HPV 16 + HSIL (n = 19) and HPV 16 + CSCC (n = 22) tissues. It was found that the expressions of all three circRNAs were significantly up-regulated in CSCC compared with those in NCE and HSIL (all $P < 0.05$), except for circRP13-279N23.2 between HSIL and CSCC with HPV16+ (Fig. 1K–M). Then, we expanded HSIL (n = 46) and CSCC (n = 48) samples with all positive HPV types for further validation, and found that the results were similar as in samples with HPV16+ alone (Fig. 1N–P). Notably, circPOLD1 expression was significantly up-regulated from NCE throughout HSIL to CSCC tissues (all $P < 0.05$, Fig. 1P). Thus, we selected circPOLD1 for further study.

Identification of circPOLD1 as a circular RNA

CircPOLD1 has been included in CircBase as has_circ_0052012, but its function remains unknown up to date, to our knowledge. To verify that exon 2 and 3 of the POLD1 gene form a circular RNA, we designed divergent primers to specifically amplify the back-spliced junction of circPOLD1, which was validated by sanger sequencing (Fig. 2A). CircPOLD1 from cervical cancer cells, SiHa and CaSki, was treated with RNase R, which digests linear RNAs, but not circular RNAs, and turned out to be stable to RNase R digestion (Fig. 2B). Then we designed convergent primers that amplified the linear POLD1 mRNA, which is the canonical form of POLD1. The convergent primers amplified products both in genomic DNA and complementary DNA, while the divergent primers only amplified the products in complementary DNA (Fig. 2C). Two pairs of full-length divergent primers were designed in two different sites of circPOLD1. The whole sequence of circPOLD1 were amplified by reverse transcription-PCR and verified with sanger sequencing (Fig. 2D). Northern blot assay using junction-specific probe further confirmed that circPOLD1 existed in SiHa cells and resisted to RNase R digestion (Fig. 2E). Fluorescent in situ hybridization assay with junction-specific probe was conducted to demonstrate the subcellular localization of circPOLD1, and showed that circPOLD1 was densely in cytoplasm and faintly in nucleus of SiHa and CaSki cells (Fig. 2F).

CircPOLD1 knockdown suppresses the survival and proliferation in cervical cancer cells

To explore the function of circPOLD1 in cervical cancer cells, two siRNAs targeting the back-spliced junction of circPOLD1 were established to knockdown circPOLD1 in SiHa and CaSki cells (Fig. 3A). After the siRNAs were transfected, circPOLD1 expression was significantly

(See figure on next page.)

Fig. 1 The profiles and identification of differentially expressed circRNAs in cervical squamous-cell carcinoma and precursor tissues. **A** The box plot of the FPKM of 24 sequencing samples. **B** The numbers of differentially expressed circRNAs between two groups. **C**–**H** Volcano plots represented differentially expressed circRNAs between two groups. The red and blue dots represent up- and down- regulated circRNAs, respectively, by at least onefold significantly (P-values < 0.05). **I** Overlap of upregulated circRNAs in HSIL and CSCC group compared with HPV-NCE group. **J** Overlap of upregulated circRNAs in HSIL and CSCC group compared with HPV16+ NCE group. **K**–**M** Relative expression levels of circRP13-279N23.2, circSTAG1 and circPOLD1 measured by qRT-PCR in HPV-NCE (n = 32), HPV16+ HSIL (n = 19) and HPV16+ CSCC (n = 22) group. In each assay, the scatter plot represents median with interquartile range (*P < 0.05, **P < 0.01, ***P < 0.001, Kruskal–Wallis test). **N**–**P** Relative expression levels of circRP13-279N23.2, circSTAG1, and circPOLD1 measured by qRT-PCR in HPV-NCE (n = 32), HSIL with all-type HPV positive (n = 46), and CSCC with all-type HPV positive (n = 48) group. In each assay, the scatter plot represents median with interquartile range (*P < 0.05, **P < 0.01, ***P < 0.001, Kruskal–Wallis test)

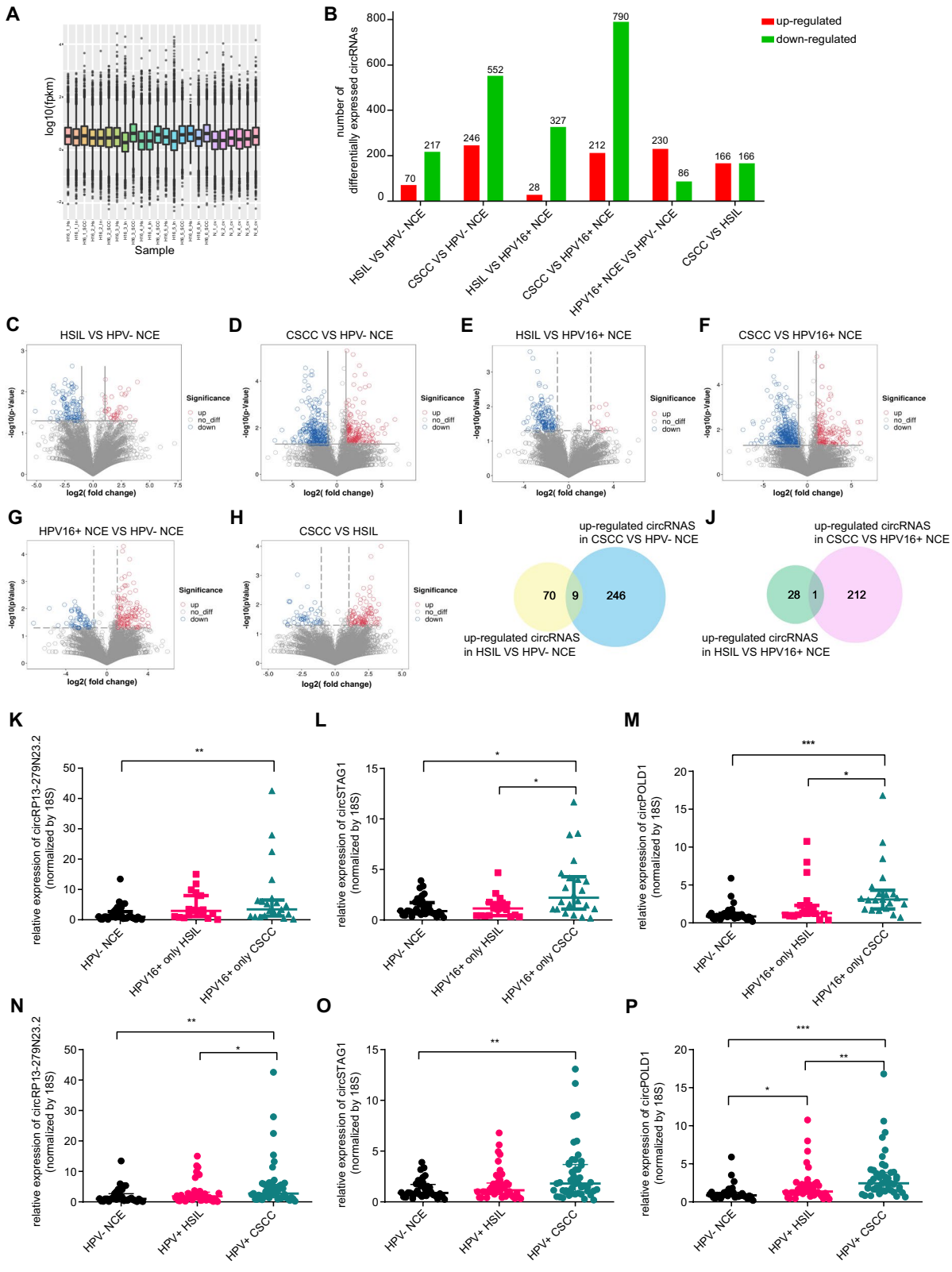

Fig. 1 (See legend on previous page.)

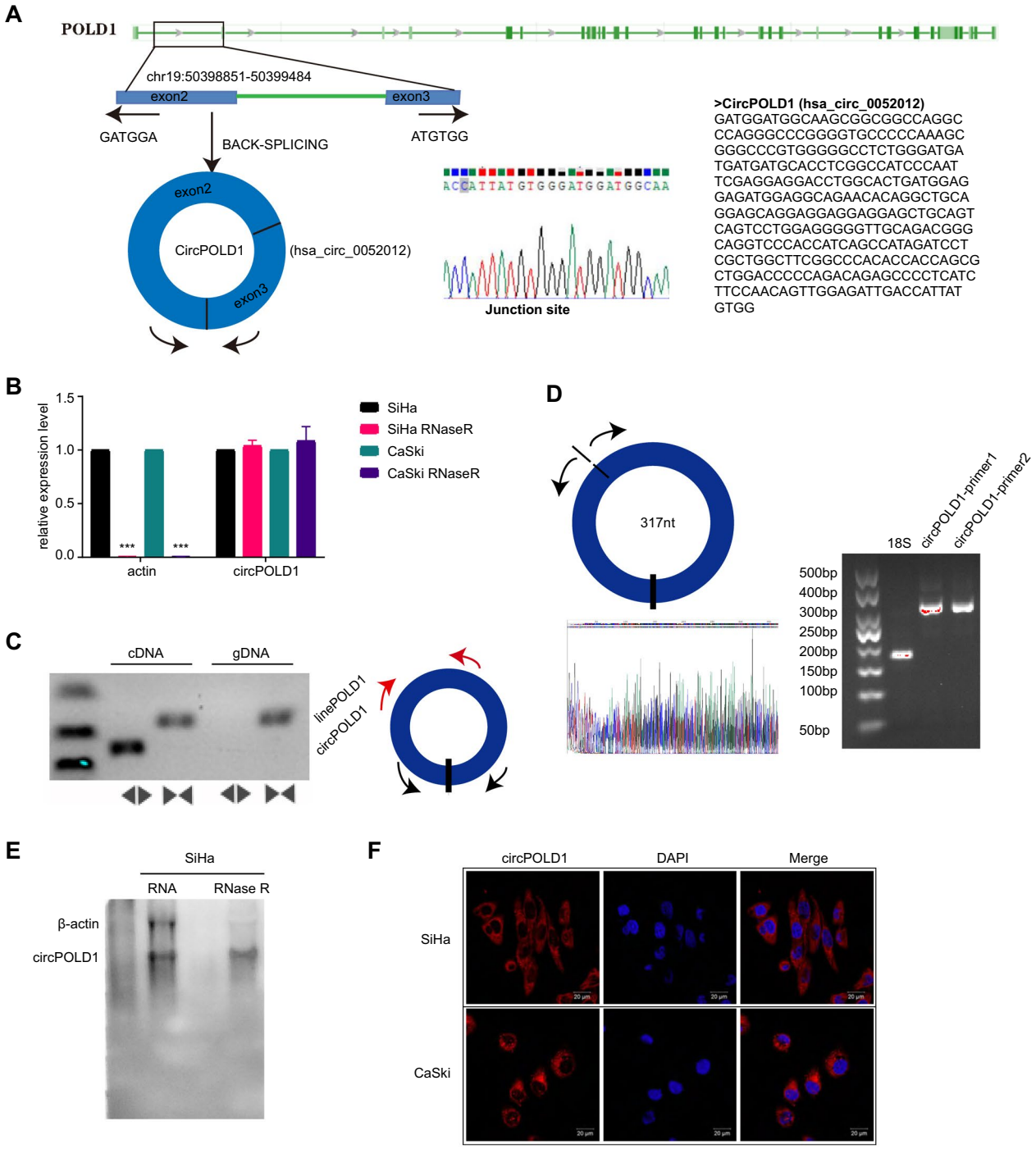

Fig. 2 Identification of circPOLD1 as a circular RNA. **A** The genomic loci of POLD1 gene and circPOLD1. Sanger sequencing of qRT-PCR product of circPOLD1 showed the back-spliced junction. **B** The qRT-PCR analysis of circPOLD1 after treated with RNase R in SiHa and CaSki cells (***$P < 0.001$, Student's t-test). **C** CircPOLD1 was validated by RT-PCR using divergent and convergent primers in complementary DNA (cDNA) and genomic DNA (gDNA) in SiHa cells. **D** The sequence of circPOLD1 was obtained from sanger sequencing (left). PCR products of circPOLD1 with two pairs of divergent primers that amplified the whole sequence of circPOLD1 in SiHa cells (right). **E** The circPOLD1 expression measured by Northern blot in RNA of SiHa cells treated with or without RNase R digestion, respectively. Probe of β-actin was incubated in the same membrane as control. **F** The circPOLD1 subcellular localization in SiHa and CaSki cells measured by fluorescent in situ hybridization assay. CircPOLD1 was labeled with a specific probe (red) for the back-splice junction, and the nucleus was labeled with DAPI (blue)

decreased (all $P < 0.01$), while POLD1 mRNA expression remained unchanged (Fig. 3B), suggest that the siRNAs are specific to circPOLD1. CCK8 assays demonstrated that circPOLD1 knockdown remarkably inhibited the proliferation in SiHa and CaSki cells (Fig. 3C). Colony formation assays showed that circPOLD1 knockdown significantly reduced the colony forming efficiency of SiHa and CaSki cells (Fig. 3D). In addition, flow cytometry showed that circPOLD1 knockdown induced apoptosis in SiHa and CaSki cells (Fig. 3E).

To further explore the effects of circPOLD1 on tumor growth in vivo, we established stable circPOLD1 knockdown SiHa cell lines (Fig. 3F). Stable circPOLD1 knockdown and control SiHa cells were subcutaneously injected into the nape of 12 BALB/c female nude mice, respectively, to establish the xenograft models. Compared with the control group, the volume and growth rate of xenografts were significantly declined in circPOLD1 stably knockdown group (all $P < 0.05$) (Fig. 3G).

CircPOLD1 promotes the proliferation through directly binding to YBX1 in cervical cancer cells

It has been demonstrated that circRNA is able to bind to RNA-associated proteins to form RNA–protein complex that regulates gene transcription [13]. We utilized the online web server RBPmap, and found multiple proteins that might be bound to circPOLD1, including YBX1 (Fig. 3H), which has been identified to bind to various non-coding RNAs [24, 25]. RNA pull-down assays using biotinylated junction-specific probe of circPOLD1 were performed. The qRT-PCR showed that the circPOLD1 probe specifically pulled down circPOLD1 (Fig. 3I), and Western blot confirmed that YBX1 was precipitated by circPOLD1 (Fig. 3J). Further, we conducted RNA immunoprecipitation in SiHa cells to pull down circPOLD1 using the anti-YBX1 antibody, followed by qRT-PCR. As we expected, circPOLD1 expression was significantly higher in the anti-YBX1 group than that in control IgG group (Fig. 3K). Our results suggest that circPOLD1 binds directly to YBX1 in cervical cancer cells.

We further knockdown YBX1 in SiHa and CaSki cells (Fig. 3L), and found by CCK8 and colony formation assays that YBX1 knockdown inhibited the proliferation of SiHa and CaSki cells significantly (Fig. 3M, N), just as circPOLD1 did. The rescue experiments were performed by establishing a co-transfection system of down-regulating circPOLD1 expression by siRNA and up-regulating YBX1 expression by plasmid in CaSki cells simultaneously (Fig. 3O). The qRT-PCR assays showed that circPOLD1 knockdown significantly downregulated the expression of CDC25A, CIAPIN1 and XIAP, which are the target genes of YBX1 and act as proliferation promoters in cancer [26], but the overexpression of YBX1 abolished this effect induced by circPOLD1 knockdown

(See figure on next page.)

Fig. 3 CircPOLD1 promotes the proliferation through directly binding to YBX1 in cervical cancer cells. **A** Schematic representation of the sites of the siRNAs specific to the back-splice junction of circPOLD1. **B** The circPOLD1 and POLD1 mRNA expression measured by qRT-PCR analysis in SiHa and CaSki cells after transfected with two siRNAs. Data were the means ± SEM of three independent experiments (*P < 0.05, **P < 0.01, ***P < 0.001, Student's t-test). **C** The proliferation measured by CCK-8 assay in SiHa and CaSki cells transfected with circPOLD1 siRNAs, oligo control (oligo) and without treated (wildtype). Data were the means ± SEM of three experiments (*P < 0.05, **P < 0.01, ***P < 0.001, Student's t-test). **D** Representative image (left) and quantification (right panel) of colony formation assays in SiHa and CaSki cells transfected with circPOLD1 siRNAs or oligo control. Data were the means ± SEM of three experiments (*P < 0.05, **P < 0.01, Student's t-test). **E** Apoptotic rates measured by flow cytometry in SiHa and CaSki cells transfected with circPOLD1 siRNAs or oligo control. Data were the means ± SEM of five experiments (*P < 0.05, **P < 0.01, Student's t-test). **F** The circPOLD1 expression measured by qRT-PCR in SiHa cells after stably transfected with circPOLD1 shRNA(sh-circPOLD1) or oligo shRNA(oligo). **G** SiHa cells with stably transfected sh-circPOLD1 or oligo were subcutaneously injected into 6 BALB/c nude mice (4–6 weeks old, female), respectively, to establish the xenograft models. Top panel: The growths of xenografts were compared between sh-circPOLD1 and oligo group (*P < 0.05, **P < 0.01, ***P < 0.001, Student's t-test). Tumor volumes were measured per week. Bottom panel: The photo showed the sizes of tumors when mice were sacrificed at week 8. **H** YBX1, the circPOLD1 binding protein predicted by online web server RBPmap. **I**, **J** Probes targeting back-splice junction of circPOLD1 and control oligo were transcribed in vitro, biotinylated, captured by streptavidin magnetic beads, and incubated with CaSki whole-cell lysates for RNA pull-down assays. The expression level of RNA measured by qRT-PCR in the eluate (left). CircPLD1 specific bands were assessed by Western blotting (right). Data were the means ± SEM of three experiments (*P < 0.05, Student's t-test). **K** RIP assays were performed using antibodies against YBX1 in CaSki cells. The quantity of circPOLD1 was evaluated by qRT-PCR. Data were the means ± SEM of three experiments (*P < 0.05, Student's t-test). **L** The expression level of YBX1 protein in SiHa cells after treated with two YBX1 siRNAs. **M** The proliferation by CCK-8 assay in SiHa and CaSki cells transfected with oligo control or YBX1 siRNAs. Data were the means ± SEM of three experiments (*P < 0.05, **P < 0.01, One-way ANOVA). **N** Representative images (left) and quantification (right) of colony formation assays in SiHa and CaSki cells transfected with YBX1 siRNAs or control. Data were the means ± SEM of three experiments (*P < 0.05, **P < 0.01, One-way ANOVA). **O** Co-transfection with circPOLD1 siRNA (si-circPOLD1) and YBX1 plasmid in CaSki cells was established. Down-regulated circPOLD1 expression and up-regulated YBX1 expression were evaluated by qRT-PCR. **P** Relative mRNA expressions of three downstream target genes of YBX1 (CDC25A, CIAPIN1 and XIAP) were measured by qRT-PCR in CaSki cells treated with control vector, si-circPOLD1, and si-circPOLD1 plus YBX1, respectively. **Q** The proliferation measured by CCK8 assay in CaSki cells treated with control vector, si-circPOLD1, and si-circPOLD1 plus YBX1, respectively. **R** Representative images of colony formation assays in CaSki cells treated with control vector, si-circPOLD1 and si-circPOLD1 plus YBX1, respectively. Data were the means ± SEM of three experiments (*P < 0.05, **P < 0.01, One-way ANOVA)

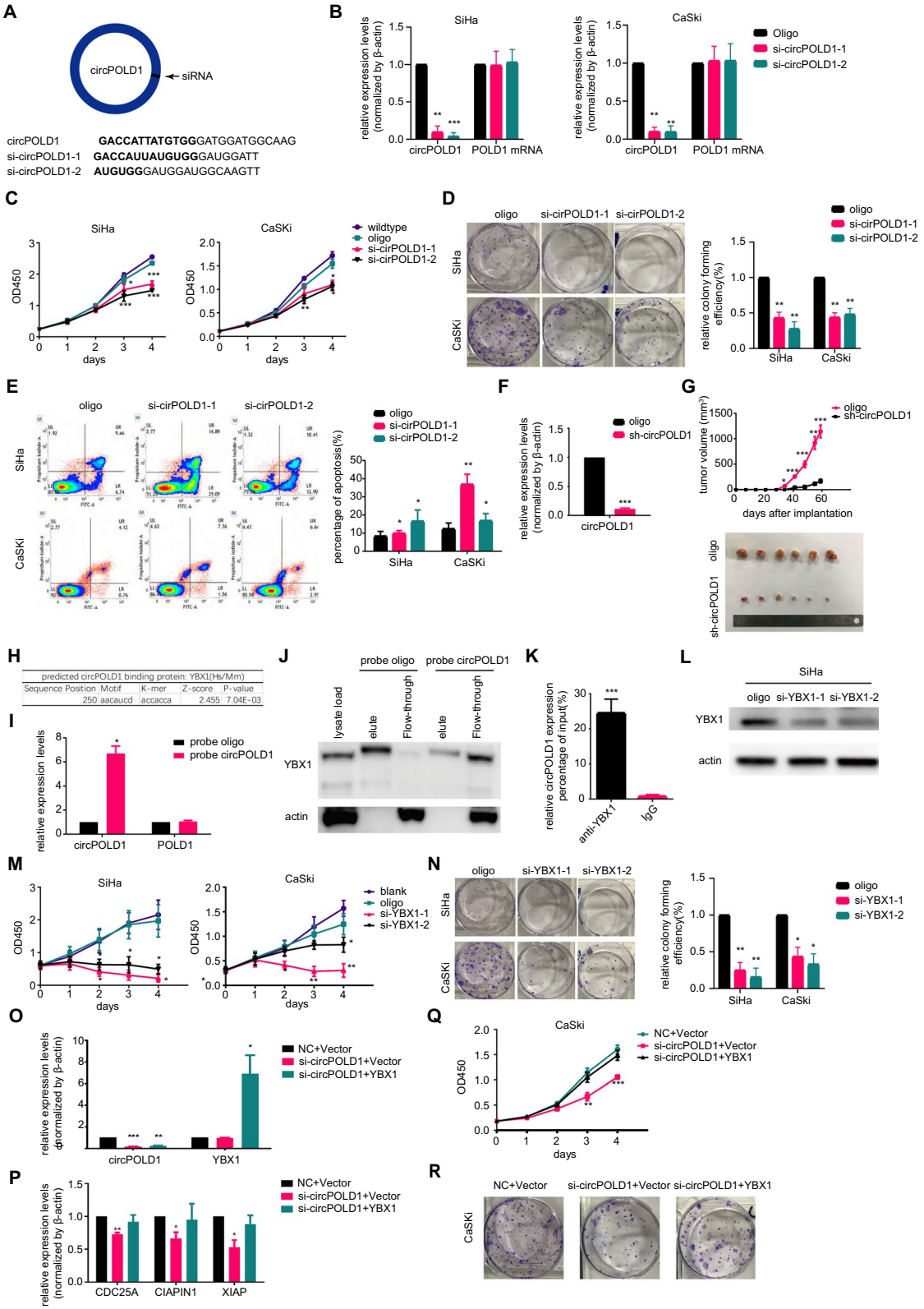

Fig. 3 (See legend on previous page.)

in CaSki cells (Fig. 3P). Moreover, CCK8 and colony formation assays also showed that overexpression of YBX1 partially resumed proliferation inhibited by circPOLD1 knockdown in CaSki cells (Fig. 3Q, R). Our results suggest that circPOLD1 promotes the proliferation through directly binding to YBX1 in cervical cancer cells.

CircPOLD1 regulates AKT/mTOR/HIF-1α and glycolysis signaling pathway through phosphorylating YBX1 in cervical cancer cells

To further investigate the mechanism of circPOLD1 in cervical cancer carcinogenesis via directly binding to YBX1, we firstly detected the expression of YBX1 in circPOLD1 knockdown cells. As shown in Fig. 4A and B, the YBX1 protein levels did not change significantly with circPOLD1 regulation. Previous study indicated that YBX1 could be phosphorylate at serine 102 to activate downstream oncogenic target molecules in tumor progression [27]. As expected, the expression level of p-YBX1 (s102) reduced with circPOLD1 knockdown in CaSki and SiHa cells (Fig. 4A and B). In addition, transcriptomics analysis was conducted on circPOLD1 and YBX1 knockdown cells constructed by two siRNAs sequences as well as the control cells. The RNA sequencing analysis yielded 34 differentially expressed genes showed a consistent expression trend in si-YBX1 and si-circPOLD1 cells compared with the si-NC cells (Fig. 4C). Of the overlap genes, cluster heatmap displayed that 14 protein coding genes were downregulated and 16 protein coding genes were upregulated following YBX1 and circPOLD1 knockdown (Fig. 4D). Moreover, the pathway enrichment analysis of overlapping differential genes were identified the glycolysis/gluconeogenesis as the most significant associated pathway both in circPOLD1 knockdown and YBX1 knockdown cells, which might act a downstream signaling regulated by circPOLD1 binding to YBX1 (Fig. 4E). Thus, the overlap downregulated differential gene LDHA expression was evaluated after knockdown circPOLD1 and YBX1, besides, other critical factors of glycolysis HK2 and HIF-1α expression were also detected. The western blot assay showed the expression of LDHA, HK2, and HIF-1α were significantly downregulation both by circPOLD1 knockdown and YBX1 knockdown in CaSki and SiHa cells (Fig. 4F and G). The AKT/mTOR signaling is confirmed to be regulated HIF-1α dependent glycolysis pathway [28]. Indeed, the level of phosphorylated AKT and mTOR were also restrained in CaSki and SiHa cells with circPOLD1 and YBX1 inhibition (Fig. 4H and I). These results suggested that circPOLD1 activated AKT/mTOR/HIF-1α and glycolysis signaling pathway via YBX1 phosphorylation.

The biomarker potential of circPOLD1 and YBX1 in cervical carcinogenesis

To explore the clinical significance of circPOLD1 detection, we further made TMAs by collecting FFPE tissues of NCE (n = 81), LSIL (n = 169), HSIL (n = 187), and CSCC (n = 253). Basescope and immunohistochemistry were performed using the TMAs to determine the expression of circPOLD1 and YBX1, respectively. Figure 5A showed representative BaseScope images of circPOLD1 and immunohistochemistry images of YBX1 in the TMAs. CircPOLD1 signals were recognized as relatively small red dots located in cells. Remarkably, the BaseScope signal of circPOLD1 was almost negative in NCE tissues, significantly higher in LSIL than that in NCE tissues ($P = 0.004$), significantly higher in HSIL than that in LSIL tissues ($P < 0.001$), and also higher, but not significantly, in CSCC than that in HSIL tissues (Fig. 5B). Similarly, the levels of YBX1 expression were significantly higher in CSCC than that in HSIL tissues ($P < 0.001$), significantly higher in HSIL than that in LSIL tissues ($P < 0.001$), and also significantly higher in LSIL than that in NCE tissues ($P < 0.001$, Fig. 5B). Further, there was a statistically positive correlation between circPOLD1 and YBX1 expressions (Fig. 5C $R = 0.497$, $P < 0.001$). We then utilized principal component analysis to make a circPOLD1/YBX1 multi-marker panel for LSIL+ and HSIL+ identification, respectively. The ROC curve of circPOLD1/YBX1 panel achieved larger area under curve (AUC) than that of single circPOLD1 detection to identify LSIL+ (LSIL or worse) and HSIL+ (HSIL and

(See figure on next page.)

Fig. 4 CircPOLD1 regulates AKT/mTOR/HIF-1α and glycolysis signaling pathway through phosphorylating YBX1 in cervical cancer cells. **A**, **B** Left panel: The YBX1 and p-YBX1 protein expression in CaSki and SiHa cells transfected with circPOLD1 siRNAs or control through western blot. Right panel: The quantitative analysis of YBX1 and p-YBX1 protein expression by ImageJ (**P < 0.01, ***P < 0.001, One-way ANOVA). **C** Venn diagram showing the overlap differentially genes between si-YBX1 vs si-NC and si-circPOLD1 vs si-NC via RNA sequencing. **D** The cluster heatmap of overlap differentially expressed mRNAs in YBX1 and circPOLD1 knockdown or control cells. **E** The pathway enrichment analysis of overlapping differential genes between si-YBX1 vs si-NC and si-circPOLD1 vs si-NC via RNA sequencing. **F** Protein levels of YBX1, p-YBX1, LDHA, HK2, HIF-1α, mTOR, p-mTOR, AKT and p-AKT, were determined following transfection with two YBX1 siRNAs and si-NC in CaSki and SiHa cells. **G** The quantitative analysis of **F** by ImageJ (*P < 0.05, **P < 0.01, ***P < 0.001, One-way ANOVA). **H** Protein levels of LDHA, HK2, HIF-1α, mTOR, p-mTOR, AKT and p-AKT were determined following transfection with two circPOLD1 siRNAs and si-NC in CaSki and SiHa cells. **I** The quantitative analysis of **H** by ImageJ (**P < 0.01, ***P < 0.001, One-way ANOVA)

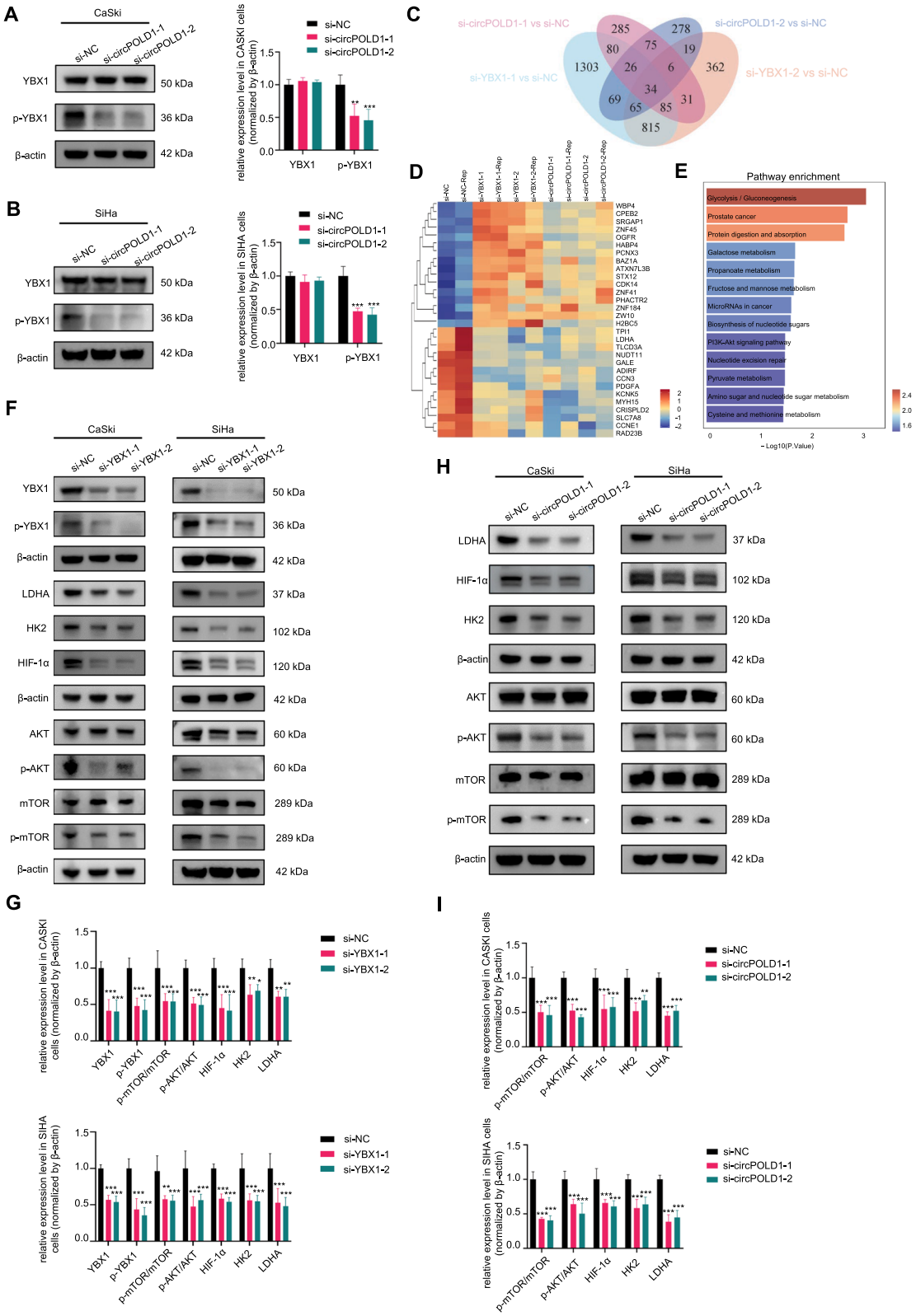

Fig. 4 (See legend on previous page.)

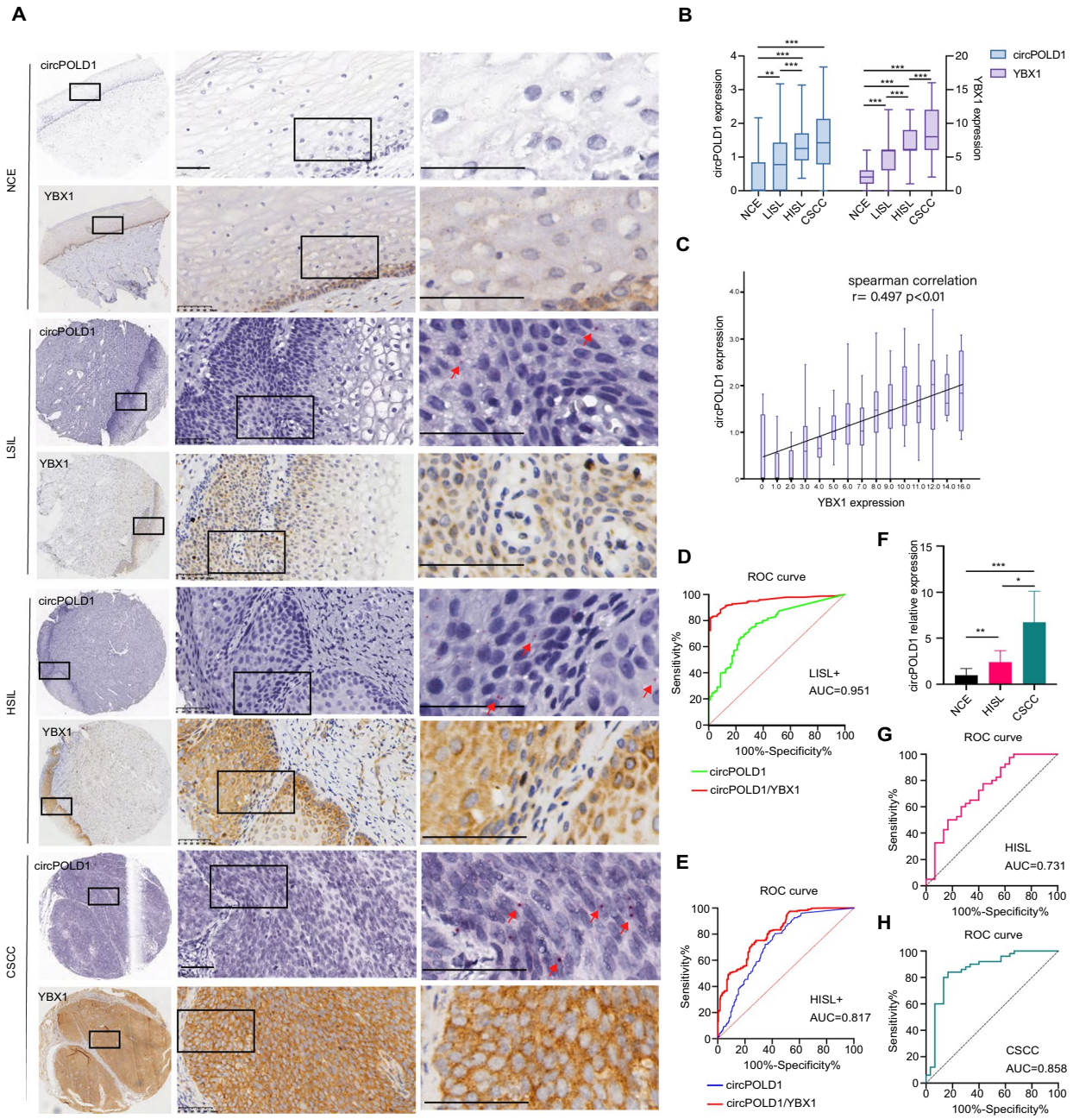

Fig. 5 The biomarker potential of circPOLD1 in cervical carcinogenesis. **A** Reprehensive images of BaseScope staining of circPOLD1 (red arrows) and immunohistochemical staining of YBX1 expression in NCE, LSIL, HSIL, and CSCC tissues. The scale bar represents 50 um. **B** Statistics analysis of density of circPOLD1 BaseScope signals and immunohistochemical detection of YBX1 expression in NCE (n = 81), LSIL (n = 169), HSIL (n = 187) and CSCC (n = 253) tissues (*P < 0.05, **P < 0.01, ***P < 0.001, Kruskal–Wallis Test). **C** Box plot analysis on NCE, LSIL, HSIL and CSCC tissues (n = 690) demonstrated the significant Spearman correlation between circPOLD1 and YBX1 expressions (r = 0.497 (95% confidence interval = 0.4365 to 0.5524), p < 0.0001). **D** In identifying LSIL + (LSIL and worse), the ROC curves of circPOLD1 (area under curve, AUC = 0.7656, P < 0.0001) and circPOLD1/YBX1panel (AUC = 0.9514, P < 0.0001). **E** In identifying HSIL + (HSIL and worse), the ROC curves of circPOLD1 (AUC = 0.7282, P < 0.001) and circPOLD1/YBX1 panel (AUC = 0.8165, P < 0.0001). **F** The relative expression of cirPOLD1 in serum specimens of an independent validation set comprising 30 normal controls, 40 HSIL patients and 50 cervical cancer patients by qRT-PCR validation. **G** The diagnostic performance of HSIL diagnosis by circPOLD1 in the serum-based validation set via ROC analysis. (AUC = 0.731, P = 0.001). **H** The diagnostic performance of cervical cancer diagnosis by circPOLD1 in the serum-based validation set. (AUC = 0.858, P < 0.0001)

worse). To identify LSIL+, the circPOLD1/YBX1 panel achieved AUC of 0.951 (P < 0.0001) with sensitivity of 0.821 and specificity of 0.988 (Fig. 5D). Similarly, to identify HSIL+, the circPOLD1/YBX1 panel achieved AUC of 0.817 (P < 0.0001) with sensitivity of 0.752 and specificity of 0.720 (Fig. 5E), suggesting the biomarker potential of circPOLD1 and YBX1 to identify cervical cancer and precursor. Moreover, circPOLD1 was significantly associated with lymph node metastasis (Table 1) by analysis of patients' clinicopathological parameters, which has been established as an independent prognostic factor in cervical carcinoma, suggesting their value in clinical outcomes. Additionally, we collected a set of serum samples, including normal controls (n = 30), HISL (n = 40), and cervical cancer patients (n = 50) to detect the ability of circPOLD1 in liquid biopsy. The results showed that the expression of circPOLD1 was gradually increased in serum of HISL and cervical cancer patients compared with normal controls (Fig. 5F). Moreover, the ROC curve of circPOLD1 was analyzed to evaluate its ability for HISL and cervical cancer identification. The circPOLD1 panel achieved AUC of 0.731 to identify HISL, with sensitivity of 0.775 and specificity of 0.567 (Fig. 5G), and AUC of 0.858 for CSCC, with sensitivity of 0.840 and specificity of 0.833 (Fig. 5H), suggesting the potential ability of circPOLD1 to identify HSIL and cervical cancer in liquid biopsy.

Table 1 clinicopathological characteristics of patients with cervical cancer

Variable	circPOLD1 expression		P value
	Low No./ratio	High No./ratio	
Figo staging (2009)			
I	59	121	0.820
II	24	46	
Lymph node metastases			
Absent	70	125	0.015*
Present	5	29	
Histological grade			
G1	3	2	0.435
G2	60	117	
G3	16	35	
Stroma invasion			
Absent	49	82	0.156
Present	31	77	
Parametrial invasion			
Absent	75	150	0.593
Present	2	8	
Tumor diameter (cm)			
< 4 cm	72	150	0.727
≥ 4 cm	10	18	

Discussion

Cervical cancer progresses through distinct stages, from NCE to HSIL and CSCC. Despite advancements in screening methods, such as cytology and HPV testing, these methods continue to encounter significant limitations in sensitivity, specificity, and clinical applicability. Consequently, there is an urgent need to identify novel biomarkers capable of addressing these gaps, particularly for early detection and risk stratification of cervical cancer. Our study identifies circPOLD1 as a novel, stage-specific circRNA whose expression progressively increases from NCE to CSCC, making it a promising candidate for early detection and diagnosis of cervical cancer.

In contrast to previous studies focusing on circRNAs in cervical cancer [29–34], our research provides a comprehensive evaluation of the dynamic expression profile of circPOLD1 across different stages of cervical carcinigenesis. We demonstrate that circPOLD1 is significantly upregulated in HSIL and CSCC tissues compared to NCE, indicating its potential as an early biomarker of cervical cancer progression. A key novel aspect of our study lies in the mechanistic insights we provide regarding how circPOLD1 facilitates cervical cancer progression. Through functional assays, we show that circPOLD1 acts as an oncogene by binding to the RNA-binding protein YBX1, which subsequently activates the AKT/mTOR/HIF-1α signaling pathway, a key driver of glycolysis and tumor progression [35, 36]. Recent studies have demonstrated that YBX1, as an RBP, can activate downstream oncogenic pathway by interacting with circRNAs. For instance, circRNA-SORE stabilizes YBX1 to induce the expression of AKT, ERK, and Raf1 by inhibiting PRP19 in hepatocellular carcinoma [25]. Similarly, Huang et al. reported that circMAN1A2_009 binds to YBX1, promoting its nuclear localization and activation of downstream transcription targets such as GLO1 mRNA in cervical carcinogenesis [27]. Our study adds to this growing body of evidence by showing that circPOLD1 promotes YBX1 phosphorylation at serine 102, further activating downstream oncogenic pathways. Specifically, we demonstrated that the relative phosphorylation level of YBX1 was significantly reduced following circPOLD1 knockdown in CaSki and SiHa cells, indicating that circPOLD1 plays a pivotal role in regulating YBX1 activity. Notably, YBX1 knockdown in cervical cancer cells induced similar phenotypic changes to circPOLD1 downregulation, suggesting that YBX1 serves as a critical mediator of circPOLD1's oncogenic effects. Moreover, the inhibitory effects induced by circPOLD1 knockdown were partially reversed upon YBX1 overexpression, further supporting the functional interaction between circPOLD1 and YBX1.

To validate these findings, we utilized BaseScope and IHC techniques. BaseScope's high sensitivity enabled us to visualize circPOLD1 expression patterns and localize them within tissue microarrays, while IHC confirmed the elevated expression of both circPOLD1 and YBX1 across different stages of cervical cancer. Importantly, the circPOLD1/YBX1 multi-marker panel demonstrated high diagnostic performance, with an AUC of 0.951 for detecting LSIL+ and 0.817 for HSIL+ lesions. These results highlight the potential of circPOLD1 as a non-invasive biomarker for early detection, as serum circPOLD1 levels increased progressively across disease stages, supporting its application as a liquid biopsy marker.

Our study further emphasizes the clinical relevance of circPOLD1 as a novel biomarker for cervical cancer screening. Conventional screening methods, such as cytology and HPV testing, remain limited by factors such as sample quality, interobserver variability, and lack of specificity, which often lead to unnecessary follow-up procedures, including colposcopy and biopsy [7]. In contrast, circRNAs inculding circPOLD1, offer several advantages, including high stability, tissue-specific expression, and potential application in liquid biopsy, making them ideal candidates for dynamic monitoring and prognostic assessment [12, 13, 16]. Our findings suggest that circPOLD1, in combination with YBX1, can optimize the sensitivity–specificity trade-off inherent to conventional cervical cancer screening methods, potentially reducing overtreatment and improving clinical outcomes.

The molecular mechanism underlying the role of circPOLD1 in cervical carcinogenesis is also noteworthy. By interacting with YBX1, circPOLD1 not only enhances the stability and nuclear localization of YBX1 but also promotes its phosphorylation, thereby activating downstream oncogenic pathways. Specifically, our study demonstrates that circPOLD1-mediated YBX1 phosphorylation results in the activation of the AKT/mTOR/HIF-1α pathway, a critical driver of glycolysis and tumor progression [35, 36]. This finding highlights the complex and multifaceted nature of circRNAs and their capacity to influence cancer metabolism, a key hallmark of tumorigenesis.

While our findings are promising, further research is warranted to validate the clinical utility of circPOLD1 as a biomarker for cervical cancer risk stratification and early detection. Future directions will include expanding the clinical validation of circPOLD1 across larger and more diverse cohorts, as well as evaluating its role in post-screening management. Additionally, mechanistic studies exploring the interaction between circPOLD1, YBX1, and other potential binding partners will provide a more comprehensive understanding of the molecular pathways driving cervical cancer progression.

Conclusion

Our study identifies circPOLD1 as a novel, stage-specific biomarker that plays a pivotal role in cervical cancer progression. We provide compelling evidence that circPOLD1 promotes tumorigenesis by interacting with YBX1 and activating the AKT/mTOR/HIF-1α signaling pathway. The combination of circPOLD1 and YBX1 detection in both tissue and serum samples significantly enhances the diagnostic accuracy for cervical cancer and its precursors, presenting a promising approach for improving early detection and reducing the burden of cervical cancer through targeted interventions. Moreover, the integration of novel RNA in situ hybridization technologies and liquid biopsy approaches positions circPOLD1 as a valuable tool for clinical practice, paving the way for the future development of non-invasive, highly sensitive screening methods for cervical cancer.

Materials and methods

Human tissue samples

All the samples were collected from patients who underwent treatment at Women's hospital, Zhejiang University School of Medicine, China. Patients were informed consent for obtaining samples and the study was approved by the Hospital Ethical Committee and conducted in accordance with the 2008 Declaration of Helsinki. HPV negative normal cervical epithelium (HPV− NCE) and HPV16 positive normal cervical epithelium (HPV16+ NCE) were collected from patients who underwent total hysterectomy for benign uterine conditions such as uterine fibroids at our hospital, HPV16+ high-grade squamous intraepithelial lesion (HSIL) were obtained from colposcopy-guided biopsies, loop electrosurgical excision procedures (LEEP), or cold knife conization, and HPV16+ cervical squamous-cell carcinoma samples (CSCC) tissues were obtained from patients following cervical cancer surgery. All tissues were diagnosed by clinical histopathology. Additional criteria: Age 25–70 years and with complete clinicopathological records. Exclusion Criteria: (1) History of other malignant tumors. (2) Concurrent viral infections other than hepatitis B virus (HBV) (e.g., syphilis, HIV). (3) Other patients who are not eligible (e.g., Comorbid autoimmune diseases or Current pregnancy). On the basis of previous researches [37], six samples of each group were collected for circRNA high-throughput sequencing analysis to ensure the reliability and accuracy of study. Moreover, 32 HPV− NCE, 46 HSIL (HPV16+ or other types positive) and 48 CSCC (HPV16+ or other types positive) tissues were obtained for validation by qRT-PCR assays. In addition, totally

1058 formalin-fixed, paraffin embedded (FFPE) tissue blocks from 690 patients including 81 of NCE, 169 of low-grade squamous intraepithelial lesion (LSIL), 187 of HSIL, and 253 of CSCC, were collected to construct tissue microarrays (TMAs). The peripheral blood samples include 40 HSIL patients, 50 cervical cancer patients and 30 non-disease controls were obtained from August 2022 to December 2023 for evaluating biomarkers into a blood-based detection. The peripheral blood specimens were subjected to centrifugation at 3000 rpm for 10 min, after which the resulting supernatant was aliquoted and cryopreserved at −80 °C in preparation for subsequent total RNA isolation procedures.

Identification of HPV genotype

Exfoliated cells of each tissue sample were collected by collection brushes and tubes for HPV genotyping test. And HPV types were tested by 21 HPV GenoArray Diagnostic innovation technologies (Hybribio Company, China). As there may be false negative results for the detection using above technologies, nested PCR was performed to amplify a part of the HPV L1 gene, which encodes the major capsid protein of several subtypes of HPV. DNA from each HPV negative exfoliated cell sample tested by above technologies was amplified with the consensus primers MY09/ MY11 followed by amplification with general primers GP5+/GP6+ by two-step nested PCR to further verify if the specimens were truly HPV negative. Co-amplification with the human β-globin primers GH20/PC04 was performed as an internal reaction control.

Establishment of sequencing libraries for detecting circRNAs

Total RNA was isolated and purified using Trizol reagent (Invitrogen, Carlsbad, CA, USA) following the manufacturer's procedure. The RNA amount and purity of each sample was quantified using NanoDrop ND-1000 (NanoDrop, Wilmington, DE, USA). The RNA integrity was assessed by Agilent 2100 with RNA number >7.0. Approximately 5 ug of total RNA were used to deplete ribosomal RNA according to the manuscript of the Ribo-Zero™ rRNA Removal Kit (Illumina, San Diego, USA). After removing ribosomal RNAs, the left RNAs were fragmented into small pieces using divalent cations under high temperature. Then the cleaved RNA fragments were reverse-transcribed to create the cDNA, which were next used to synthesize U-labeled second-stranded DNAs with *E. coli* DNA polymerase I, RNase H and dUTP. An A-base was then added to the blunt ends of each strand, preparing them for ligation to the indexed adapters. Each adapter contained a T-base overhang for ligating the adapter to the A-tailed fragmented DNA. Single-or dual-index adapters were ligated to the fragments, and size selection was performed with AMPureXP beads. After the heat-labile UDG enzyme treatment of the U-labeled second-stranded DNAs, the ligated products were amplified with PCR by the following conditions: initial denaturation at 95 °C for 3 min, 8 cycles of denaturation at 98 °C for 15 s, annealing at 60 °C for 15 s, and extension at 72 °C for 30 s, and then final extension at 72 °C for 5 min. The average insert size for the final cDNA library was 300 bp (± 50 bp). At last, the paired-end sequencing was performed on an Illumina Hiseq 4000 (LC Science Co., LTD., China) following the vendor's recommended protocol.

Bioinformatic methods for identifying circRNAs

Firstly, Cutadapt (1.10) was used to remove the reads that contained adaptor contamination, low quality bases and undetermined bases. Then sequence quality was verified using FastQC (0.10.1) (http://www.bioinformatics.babraham.ac.uk/projects/fastqc/). Bowtie2 (2.2.0) [38] and tophat2 (2.0.10) [39] was used to map reads to the genome (GRCh38) of species (Homo sapiens). Remaining reads (unmapped reads) were still mapped to genome using tophat-fusion (2.1.0) [40]. CIRCExplorer (1.0) [41, 42] was used to de novo assemble the mapped reads to circular RNAs at first; Then, back splicing reads were identified in unmapped reads by tophat-fusion. All samples were generated unique circular RNAs. The unit of measurement for circRNAs is Fragment Per Kilobase of exon per Million fragments mapped (FPKM). The differentially expressed circRNAs were selected with log2 (fold change) ≥ 1 or log2 (fold change) ≤ −1 and with statistical significance (p value < 0.05) by t test, p value is corrected using BH [43] method.

RNA extraction and real-time quantitative RT-PCR

Total RNA was extracted and purified with Trizol reagent (Invitrogen, Carlsbad, CA, USA) according to the manufacturer's instructions. The RNA amount and purity of each sample was quantified with NanoDrop ND-1000 (NanoDrop, Wilmington, DE, USA). For the RNA of tissue samples used for qRT-PCR assay, the RNA integrity was assessed by Agilent 2100 to exclude RNA samples with weak RNA integrity and ensure the accuracy of using 18S as internal reference. And 1 ug total RNA was reverse transcribed into cDNA in a reaction volume of 20 μl utilizing PrimeScript RT reagent Kit with gDNA Eraser (Takara Otsu, Shiga, Japan). QRT-PCR analyses were performed with SYBR Premix Ex Taq (Takara). All the primers used were presented in Table S1.

Cell line culture

Human cervical cancer SiHa cell line was obtained from the American Type Culture Collection (ATCC, USA). Human cervical cancer CaSki cell line was obtained from Cell resource center, Shanghai Institute of Life Sciences, Chinese Academy of Sciences (China). SiHa cells were cultured in DMEM (BI, Israel) supplemented with 10% FBS and CaSki cells were cultured in RPMI-1640 (BI, Israel) supplemented with 10% FBS, which both maintained at 37 °C in 5% CO_2.

RNA fluorescence in-situ hybridization (FISH)

CY3 labeled probe (Table S1) specifically targeting the back-spliced junction of circPOLD1 was synthesized by GeneSeed Biotech., Ltd (Guangzhou, China). SiHa and CaSki cells were seeded on the slides at the bottom of the Petri dishes and incubated. After permeabilization with 0.5% tritonx-100 and fixation with 4% paraformaldehyde, cells were incubated at 37 °C overnight in the hybridization buffer containing diluted denatured probe. Subsequently, the slides were washed and dyed with DAPI-Antifade, and finally sealed with rubber cement. Representative images for the RNA FISH were taken by Laser confocal microscope (TCS SP2 AOBS).

RNaseR resistance assay

Total RNA was incubated with or without 2U/ug Ribonuclease R (RNase R) (Epicentre, Madison, WI, USA) at 37 °C for 15 min, and then purified and recovered with RNeasy MinElute Cleanup kit (Qiagen, German) following the manufacturer's instruction.

Northern blot

The DNA probes targeting the back-spliced junction of circPOLD1 was synthesized and labeled with digoxigenin (DIG, Table S1). About 15 μg of total RNAs was denatured in formaldehyde and then separated on 1% agarose–formaldehyde gel by electrophoresis at 25 V overnight. The RNAs were then transferred to Hybond-N+ membrane (Amersham, UK, RPN303B) and hybridized with biotin labeled DNA probes at 50 °C overnight after the prehybridization at 50 °C for 2 h in DIG Easy Hyb solution (Roche, Swiss). The membrane was washed stringently, blocked in blocking solution and stained with anti-DIG antibody. Finally, the blots were exposed with X-ray films with chemiluminescence substrate CSPD (Roche, Swiss).

Western blot

Protein was extracted using RIPA lysis buffer (Solarbio, Beijing, China) with proteinase inhibitor and quantified by a BCA kit (Beyotime Biotechnology, Shanghai, China). 20 μg of total protein was separated using 4–20% SurePAGE (GenScript, USA, M00665) and transferred to polyvinylidene difluoride membrane (Bio-Rad, USA, 1620177). The membranes were blocked by 5% skim milk and then incubated overnight at 4 °C with antibodies against YBX1(Santa cruz, USA: sc-101198, 1:500), phosphoS102-YBX1 (abcam, USA: ab138654, 1:700), mTOR (CST, USA: 2983, 1:1000), phospho-mTOR (CST, USA: 2971, 1:1000), AKT (CST, USA: 9272, 1:1000), phospho-AKT (CST, USA: 4060, 1:1000), HIF-1α (Proteintech, China: 20960-1-AP, 1:2000), HK2 (Proteintech, China: 22029-1-AP, 1:5000), LDHA (CST, USA: 3582, 1:1000), Actin (Diagbio, China 1:1000) and GAPDH (Diagbio, China 1:1000). After incubated with the secondary antibodies (1: 5000), the membranes were detected using ECL chemiluminescence reagents (Thermo Fisher, USA) and analyzed with ImageQuant Las 4000 software.

Cell transfection

Small interference RNAs (siRNAs) that target the back-spliced junction of circPOLD1 were designed and synthesized by GenePharma (Shanghai, China). Short hairpin RNA (shRNA) specific against circPOLD1 junction site were inserted into lentiviral vector GV334 (Genechem, Shanghai, China) and transfected into cells to construct stably knockdown cell lines. For siRNA transfection, cells were precultured in six-well plate with 70% convergence, 2.5 μl siRNA and 2.5 μl DharmaFECT1 transfection reagent (Dharmacon, USA) were separately mixed with 125 μl OPTI-MEM medium and incubated for 5 min, then mixed together and incubated for 15 min. The transfection mixture was added to cell medium. Cells were collected after 48 h or 72 h for transfection efficiency verification or subsequent experiments. For plasmid transfection, the lentiviral particles were produced form 293 T cells transfection with the target plasmid based on shRNA sequence and helper plasmid, and then infected to cervical cancer cells. The stable cell lines were selected by puromycin (2 μg/ml) All the siRNAs used in this article were presented in Table S1.

Cell proliferation and apoptosis assays

Cell proliferation was detected with CCK8 assay and colony formation assay. For CCK8 assay, the cells ($4*10^3$/well) were seeded into 96-well plates and treated as designed. And then they were added with Cell Counting Kit-8 (CCK8) (DOJINDO, Japan, Cat# CK04) solution on days 0, 1, 2, 3 and 4. After 2 h of incubation at 37 °C, the absorbance at 450 nM was measured. For colony formation assay, the treated cells (500/well) were seeded into 6-well plates and incubated at 37 °C for 14 days. Colonies

were counted and analyzed after fixed with methanol and stained with 0.1% crystal violet.

To detect the cell apoptotic rates, after transfected with siRNAs or oligos for 72 h, SiHa and CaSki cells were stained using Annexin V-FITC/PI apoptosis kit (Mutisiences, China, AP101-100-kit) and analyzed using flow cytometry (Beckman, USA).

Biotin-labeled RNA pull-down

Biotin-labeled DNA probe specifically targeting the back-spliced junction of circPOLD1 was synthesized (Table S1). RNA pull-down assay was performed using the Pierce™ Magnetic RNA–Protein Pull-Down Kit (Thermo Scientific, USA, 20164) following the manufacturer's instructions. Briefly, Cell lysates were prepared using standard lysis buffers (Thermo Scientific, USA) and biotin-labeled DNA probes were incubated with streptavidin magnetic beads. Then the cell lysates were incubated with the streptavidin magnetic beads at 4 °C overnight. The magnetic bead was thoroughly washed and the flow through fluid was collected for further experiments. The RNA bound to the magnetic bead was detected by qRT-PCR to verify if circPOLD1 was pulled down by the DNA probe. The proteins bound to the magnetic bead were separated with SurePAGE (GenScript, USA, M00665) and detected by Western Blot.

RIP

RIP assay was performed using Magna RIP™ Quad RNA-Binding Protein Immunoprecipitation Kit (Sigma-Aldrich, USA, 17-704) according to the instructions. The YBX1 antibody (Abcam, UK, ab12148) was used in the RIP assay and mouse immunoglobulin G (IgG) was used as negative control.

Tissue micro array construction

In this study, special TMAs were constructed using 1058 FFPE tissue blocks from 690 patients, which were collected from Pathology Department, Women's Hospital, Zhejiang University School of Medicine, China, between 2017–2018. Specimens of NCE, LSIL, HSIL and CSCC area confirmed by 2 independent pathologists were collected, punched from the original tissue blocks and re-embedded into new paraffin blocks for TMA. TMA blocks were cut into 4 μm sections for BaseScope Assay and immunohistochemistry.

Immunohistochemistry

After the TMAs of the FFPE tissues were deparaffinized, rehydrated, and retrieved, the slides were then incubated with a 1:600 dilution of antibody against human YBX1 (Abcam, UK, ab12148). YBX1 immunopositivity analysis was semiquantitative and defined as the presence of any specific staining in the cytoplasm and/or nucleus. Staining intensity grade was classified as: 0 for no staining, 1 for weak, 2 for moderate, 3 for strong and 4 for extremely strong. The percentage grade of total cells that were stained were classified as: 0 for < 5%, 1 for 6–25%, 2 for 26–50%, 3 for 51–75% and 4 for 76–100%. The score of YBX1 expression was obtained by multiplying the above two grades, which ranged from 0 to 16. All the samples were examined and scored by two independent pathologists.

Nude mice xenograft experiments

CircPOLD1 stably knockdown SiHa cells and control SiHa cells were used. Totally $2*10^6$ cells were resuspended in 100 μL PBS, and injected subcutaneously into the nape of 4–6 weeks old female nude mice (BALB/c), respectively, (n = 6/each group). The size of the subcutaneous tumor was measured once a week, and the mice were sacrificed under anesthesia at week 8. All the experiments were performed under the approval of Zhejiang University, China, abiding by the Guide for the Care and Use of Laboratory Animals.

RNA in-situ hybridization

The expression of circPOLD1 in cervical tissues was evaluated by in situ hybridization (ISH) using the BaseScope Detection Reagent Kit-Red (Advanced Cell Diagnostics (ACD), Newark, CA, USA), a novel and proprietary method of ISH to visualize single circRNA molecules [44], following the manufacturer's instructions. A 1ZZ ISH probe targeting the back-spliced junction of circPOLD1 (351–78nt ofNR_046402.1) was designed, termed as BA-Hs-POLD1-circRNA-E3E2 (ACD). The evaluation was accomplished by two independent pathologists without knowledge of clinical information. For each specimen, the pathologists measured the area of the exact tissue section of NCE, LSIL, HSIL or CSCC (area) and counted the numbers of red dots in the section. Then the circPOLD1 expression scores were obtained using the following algorithm: circPOLD1 expression = Ig (number/area + 1), and the unit of measurement for area is square millimeter.

Statistical analysis

Statistical analyses were performed using SPSS26.0, GraphPad Prism 8.4.3 and Anaconda Python 3.8. The Shapiro–Wilk test was performed to assess normality of the data distribution. Student's t-test and Welch's t-test were used for two groups comparison as appropriate, defined in the figure legends. For comparisons across three groups, the Kruskal–Wallis test (non-parametric ANOVA equivalent) was employed, followed by post hoc Dunn's tests with Bonferroni correction

for multiple comparisons. Spearman's rank correlation coefficient of the expression of circPOLD1 and YBX1was assessed. Principal component analysis of circPOLD1 and YBX1 expression data was done using Python. The receiver operating characteristic (ROC) curve was used to assess the performance of circPOLD1 and YBX1 detection in identifying cervical lesions. All statistical tests were two sided, and P values less than 0.05 were considered as significant.

All the primers and probes used were listed in Supplementary Table S1.

Supplementary Information

The online version contains supplementary material available at https://doi.org/10.1186/s12967-025-06494-3.

Supplementary Material 1.

Acknowledgements
Thanks for the technical support by the Central laboratory of Women's hospital school of medicine zhejiang university.

Author contributions
JX, WL and XX designed the study. LZ, XC, YZ, YC, TZ, LW, and LX performed experiments. LZ, XC, YZ, YL, XC, WL and JX did data analyses, provided technical and theoretical support. LZ, YZ and LX collected tissue specimens and clinical data. LZ and XC wrote the original manuscript. JX revised the manuscript. All authors read and approved the final manuscript.

Funding
This work was supported by the National Natural Science Foundation of China (Grant No.82072855 and No.81702552), and the Key research and development plan in Zhejiang province (No. 2020C03025).

Availability of data and materials
All data underlying this study's conclusions are available from the corresponding author upon reasonable request.

Declarations

Ethics approval and consent to participate
The study was approved by the The study was approved by the Ethics Committee of Women's Hospital, Zhejiang University School of Medicine and the Laboratory Animal Management and Ethics Committee of Zhejiang Chinese Medical University (No.10495).

Consent for publication
Not applicable.

Competing interests
The authors declare that they have no competing interests.

Author details
[1]Department of Gynecologic Oncology, Women's Hospital, School of Medicine, Zhejiang University, No.1 Xueshi Road, Hangzhou 310006, China. [2]Zhejiang Provincial Key Laboratory of Precision Diagnosis and Therapy for Major Gynecological Diseases, Women's Hospital, School of Medicine, Zhejiang University, Hangzhou, China. [3]Department of Obstetrics and Gynecology, Peking University People's Hospital, Beijing, China. [4]Zhejiang Key Laboratory of Maternal and Infant Health, Women's Hospital, School of Medicine, Zhejiang University, Hangzhou, China.

Received: 15 September 2024 Accepted: 13 April 2025
Published online: 04 May 2025

References

1. Bray F, Laversanne M, Sung H, et al. Global cancer statistics 2022: GLOBOCAN estimates of incidence and mortality worldwide for 36 cancers in 185 countries. CA Cancer J Clin May-Jun. 2024;74(3):229–63. https://doi.org/10.3322/caac.21834.
2. Bouvard V, Wentzensen N, Mackie A, et al. The IARC perspective on cervical cancer screening. N Engl J Med. 2021;385(20):1908–18. https://doi.org/10.1056/NEJMsr2030640.
3. Bi XY, Pan ZW, Liu SL, et al. A feasibility study of DNA ploidy analysis, HPV, and TCT for screening of cervical cancer: a retrospective study. Medicine (Baltimore). 2024;103(49): e40038. https://doi.org/10.1097/MD.0000000000040038.
4. Rajaram S, Gupta B. Screening for cervical cancer: choices & dilemmas. Indian J Med Res. 2021;154(2):210–20. https://doi.org/10.4103/ijmr.IJMR_857_20.
5. Rodriguez AC, Schiffman M, Herrero R, et al. Rapid clearance of human papillomavirus and implications for clinical focus on persistent infections. J Natl Cancer Inst. 2008;100(7):513–7. https://doi.org/10.1093/jnci/djn044.
6. Cao D, Yang Z, Dong S, et al. PCDHGB7 hypermethylation-based Cervical cancer Methylation (CerMe) detection for the triage of high-risk human papillomavirus-positive women: a prospective cohort study. BMC Med. 2024;22(1):55. https://doi.org/10.1186/s12916-024-03267-5.
7. Kaljouw S, Jansen EEL, Aitken CA, Harrijvan LM, Naber SK, de Kok I. Reducing unnecessary referrals for colposcopy in hrHPV-positive women within the Dutch cervical cancer screening programme: a modelling study. Gynecol Oncol. 2021;160(3):713–20. https://doi.org/10.1016/j.ygyno.2020.12.038.
8. Schreiberhuber L, Barrett JE, Wang J, et al. Cervical cancer screening using DNA methylation triage in a real-world population. Nat Med. 2024;30(8):2251–7. https://doi.org/10.1038/s41591-024-03014-6.
9. Tian X, Weng D, Chen Y, et al. Risk assessment and triage strategy of cervical cancer primary screening on HPV integration status: 5-year follow-up of a prospective cohort study. J Natl Cancer Cent. 2024;4(4):311–7. https://doi.org/10.1016/j.jncc.2024.08.001.
10. Kepsha MA, Timofeeva AV, Chernyshev VS, Silachev DN, Mezhevitinova EA, Sukhikh GT. MicroRNA-based liquid biopsy for cervical cancer diagnostics and treatment monitoring. Int J Mol Sci. 2024. https://doi.org/10.3390/ijms252413271.
11. Salta S, Lobo J, Magalhaes B, Henrique R, Jeronimo C. DNA methylation as a triage marker for colposcopy referral in HPV-based cervical cancer screening: a systematic review and meta-analysis. Clin Epigenet. 2023;15(1):125. https://doi.org/10.1186/s13148-023-01537-2.
12. Dong J, Zeng Z, Huang Y, Chen C, Cheng Z, Zhu Q. Challenges and opportunities for circRNA identification and delivery. Crit Rev Biochem Mol Biol. 2023;58(1):19–35. https://doi.org/10.1080/10409238.2023.2185764.
13. Hussen BM, Abdullah SR, Jaafar RM, et al. Circular RNAs as key regulators in cancer hallmarks: new progress and therapeutic opportunities. Crit Rev Oncol Hematol. 2025;207: 104612. https://doi.org/10.1016/j.critrevonc.2024.104612.
14. Chen L, Shan G. CircRNA in cancer: fundamental mechanism and clinical potential. Cancer Lett. 2021;505:49–57. https://doi.org/10.1016/j.canlet.2021.02.004.
15. Kristensen LS, Jakobsen T, Hager H, Kjems J. The emerging roles of circRNAs in cancer and oncology. Nat Rev Clin Oncol. 2022;19(3):188–206. https://doi.org/10.1038/s41571-021-00585-y.
16. Misir S, Wu N, Yang BB. Specific expression and functions of circular RNAs. Cell Death Differ. 2022;29(3):481–91. https://doi.org/10.1038/s41418-022-00948-7.
17. Roy S, Kanda M, Nomura S, et al. Diagnostic efficacy of circular RNAs as noninvasive, liquid biopsy biomarkers for early detection of gastric cancer. Mol Cancer. 2022;21(1):42. https://doi.org/10.1186/s12943-022-01527-7.
18. Xu C, Jun E, Okugawa Y, et al. A circulating panel of circRNA biomarkers for the noninvasive and early detection of pancreatic ductal adenocarcinoma. Gastroenterology. 2024;166(1):178–90. https://doi.org/10.1053/j.gastro.2023.09.050.
19. Han B, Chao J, Yao H. Circular RNA and its mechanisms in disease: from the bench to the clinic. Pharmacol Ther. 2018;187:31–44. https://doi.org/10.1016/j.pharmthera.2018.01.010.

20. Long F, Li L, Xie C, et al. Intergenic CircRNA Circ_0007379 inhibits colorectal cancer progression by modulating miR-320a biogenesis in a KSRP-dependent manner. Int J Biol Sci. 2023;19(12):3781–803. https://doi.org/10.7150/ijbs.85063.
21. Shen Y, Zhang N, Chai J, et al. CircPDIA4 induces gastric cancer progression by promoting ERK1/2 activation and enhancing biogenesis of oncogenic circRNAs. Cancer Res. 2023;83(4):538–52. https://doi.org/10.1158/0008-5472.CAN-22-1923.
22. Ma T, Guo J, Han J, et al. Circ_0001589/miR-1248/HMGB1 axis enhances EMT-mediated metastasis and cisplatin resistance in cervical cancer. Mol Carcinog. 2023;62(11):1645–58. https://doi.org/10.1002/mc.23605.
23. Han X, Xia L, Wu Y, Chen X, Wu X. m6A-modified circSTX6 as a key regulator of cervical cancer malignancy via SPI1 and IL6/JAK2/STAT3 pathways. Oncogene. 2025. https://doi.org/10.1038/s41388-024-03260-5.
24. Hong X, Li Q, Li J, et al. CircIPO7 promotes nasopharyngeal carcinoma metastasis and cisplatin chemoresistance by facilitating YBX1 nuclear localization. Clin Cancer Res. 2022;28(20):4521–35. https://doi.org/10.1158/1078-0432.CCR-22-0991.
25. Xu J, Ji L, Liang Y, et al. CircRNA-SORE mediates sorafenib resistance in hepatocellular carcinoma by stabilizing YBX1. Signal Transduct Target Ther. 2020;5(1):298. https://doi.org/10.1038/s41392-020-00375-5.
26. Massad LS, Einstein MH, Huh WK, et al. 2012 updated consensus guidelines for the management of abnormal cervical cancer screening tests and cancer precursors. Obstet Gynecol. 2013;121(4):829–46. https://doi.org/10.1097/AOG.0b013e3182883a34.
27. Huang Y, Wei X, Tu M, Lu W, Xu J. CircMAN1A2_009 facilitates YBX1 nuclear localization to induce GLO1 activation for cervical adenocarcinoma cell growth. Cancer Sci. 2024;115(10):3273–87. https://doi.org/10.1111/cas.16264.
28. DeBerardinis RJ, Lum JJ, Hatzivassiliou G, Thompson CB. The biology of cancer: metabolic reprogramming fuels cell growth and proliferation. Cell Metab. 2008;7(1):11–20. https://doi.org/10.1016/j.cmet.2007.10.002.
29. Xu Y, Leng K, Yao Y, et al. A circular RNA, cholangiocarcinoma-associated circular RNA 1, contributes to cholangiocarcinoma progression, induces angiogenesis, and disrupts vascular endothelial barriers. Hepatology. 2021;73(4):1419–35. https://doi.org/10.1002/hep.31493.
30. Yuan F, Tang Y, Liang H, et al. CircPIK3C3 inhibits hepatocellular carcinoma progression and lenvatinib resistance by suppressing the Wnt/beta-catenin pathway via the miR-452–5p/SOX15 axis. Genomics. 2025. https://doi.org/10.1016/j.ygeno.2025.110999.
31. Ji F, Du R, Chen T, et al. Circular RNA circSLC26A4 accelerates cervical cancer progression via miR-1287-5p/HOXA7 axis. Mol Ther Nucleic Acids. 2020;19:413–20. https://doi.org/10.1016/j.omtn.2019.11.032.
32. Zhang Y, Li X, Zhang J, et al. USF1 regulated circPRDM4 modulates tumorigenesis and immune escape in chemoresistant cervical cancer. J Cell Mol Med. 2024;28(5): e17945. https://doi.org/10.1111/jcmm.17945.
33. Heydarnia E, Dorostgou Z, Hedayati N, et al. Circular RNAs and cervical cancer: friends or foes? A landscape on circRNA-mediated regulation of key signaling pathways involved in the onset and progression of HPV-related cervical neoplasms. Cell Commun Signal. 2024;22(1):107. https://doi.org/10.1186/s12964-024-01494-0.
34. Begliarzade S, Sufianov A, Ilyasova T, et al. Circular RNA in cervical cancer: Fundamental mechanism and clinical potential. Noncoding RNA Res. 2024;9(1):116–24. https://doi.org/10.1016/j.ncrna.2023.11.009.
35. Rosic G. Cancer signaling, cell/gene therapy, diagnosis and role of nanobiomaterials. Adv Biol Earth Sci. 2024;9(1):11–34. https://doi.org/10.62476/abes9s11.
36. Montazersaheb S, Eftekhari A, Shafaroodi A, et al. Green-synthesized silver nanoparticles from peel extract of pumpkin as a potent radiosensitizer against triple-negative breast cancer (TNBC). Cancer Nanotechnol. 2024. https://doi.org/10.1186/s12645-024-00285-z.
37. Zhang Y, Zhao L, Yang S, et al. CircCDKN2B-AS1 interacts with IMP3 to stabilize hexokinase 2 mRNA and facilitate cervical squamous cell carcinoma aerobic glycolysis progression. J Exp Clin Cancer Res. 2020;39(1):281. https://doi.org/10.1186/s13046-020-01793-7.
38. Langmead B, Salzberg SL. Fast gapped-read alignment with Bowtie 2. Nat Methods. 2012;9(4):357–9. https://doi.org/10.1038/nmeth.1923.
39. Kim D, Pertea G, Trapnell C, Pimentel H, Kelley R, Salzberg SL. TopHat2: accurate alignment of transcriptomes in the presence of insertions, deletions and gene fusions. Genome Biol. 2013;14(4):R36. https://doi.org/10.1186/gb-2013-14-4-r36.
40. Kim D, Salzberg SL. TopHat-fusion: an algorithm for discovery of novel fusion transcripts. Genome Biol. 2011;12(8):R72. https://doi.org/10.1186/gb-2011-12-8-r72.
41. Zhang XO, Wang HB, Zhang Y, Lu X, Chen LL, Yang L. Complementary sequence-mediated exon circularization. Cell. 2014;159(1):134–47. https://doi.org/10.1016/j.cell.2014.09.001.
42. Zhang XO, Dong R, Zhang Y, et al. Diverse alternative back-splicing and alternative splicing landscape of circular RNAs. Genome Res. 2016;26(9):1277–87. https://doi.org/10.1101/gr.202895.115.
43. Gao Y, Wang J, Zhao F. CIRI: an efficient and unbiased algorithm for de novo circular RNA identification. Genome Biol. 2015;16(1):4. https://doi.org/10.1186/s13059-014-0571-3.
44. Nielsen BS, Moller T, Kjems J. Automated one-double-Z pair BaseScope for CircRNA in situ hybridization. Methods Mol Biol. 2020;2148:379–88. https://doi.org/10.1007/978-1-0716-0623-0_24.

Publisher's Note